

Characterization of Si nanocrystals grown by annealing SiO₂ films with uniform concentrations of implanted Si

S. Guha^{a)} and S. B. Qadri

Materials Science and Technology Division, Naval Research Laboratory, Washington, DC 20375

R. G. Musket and M. A. Wall

Materials Science and Technology Division, Lawrence Livermore Laboratory, Livermore, California 94550

Tsutomu Shimizu-Iwayama

Department of Materials Science, Aichi University of Education, Igaya-cho, Kariya-shi, Aichi 448-8542, Japan

(Received 18 January 2000; accepted for publication 11 July 2000)

We have performed physical and optical characterization of Si nanocrystals grown by ion implantation of Si⁺ ions at multiple energies with varying doses into thermally grown SiO₂ films. The purpose of multiple implants was to achieve uniform composition of the added Si profile throughout the SiO₂ film to produce Si particles with a narrow size distribution upon annealing at 1000 °C in a nitrogen atmosphere. The depth distribution of the composition and sizes of the Si particles in SiO₂ films before and after the anneal were determined using Rutherford backscattering (RBS), forward recoil spectroscopy, small-angle x-ray diffraction (SAXRD), and high-resolution transmission electron microscopy (HRTEM). From RBS we concluded that the amount of free silicon was reduced by annealing, presumably due to oxidation in the annealing process. The mean cluster sizes of the annealed samples were determined by SAXRD. HRTEM was also employed to determine the average size of Si particles. Photoluminescence spectra (PL) from these samples were broad and the peak positions of the PL spectra were blue-shifted with decreasing cluster size. The line shapes of the PL spectra were calculated with a quantum confinement model assuming a log-normal size distribution of Si nanoparticles and $(1/D)^{1.25}$ dependence of the band gap energy as a function of particle size D . The band gap energy and the average particle size obtained from the calculated line shape spectra agree well with the quantum confinement model. © 2000 American Institute of Physics. [S0021-8979(00)04020-2]

I. INTRODUCTION

In recent years, a great deal of research on Si nanocrystals (*nc-Si*) grown by various techniques¹⁻⁴ has been conducted due to its potential for application in Si-based optoelectronic devices. The key issue in the growth process is to synthesize Si nanocrystals in an insulating matrix, preferably SiO₂ films, with a narrow size distribution. This would enable one to increase the band gap of Si from 1.1 to 4 eV in small incremental energies by decreasing the particle size in small steps allowing a wide range of applications of Si as detectors, light emitting devices from infrared to visible-UV radiation, and optical interconnects compatible with the Si industry.

This work was motivated by a recent report by Shimizu-Iwayama *et al.*,⁵ in which the authors calculated that multiple implants of Si⁺ ions at different doses and energies into thermally grown, 300-nm-thick SiO₂ films would yield a very flat implant profile as compared to a single dose/single energy ion implantation that produces a Gaussian implant profile. After annealing, a single Si⁺ implant at a certain dose and energy produces a narrow band of Si nanoparticles of varying size at the peak of the Gaussian-like profile in the

SiO₂ film. In multiple implants with a flat implant profile, one expects the excess Si to be distributed uniformly throughout the oxide layers. Therefore, upon annealing at 1000 °C for 1 h in a nitrogen ambient, one would expect to observe the formation of Si nanocrystals of uniform size throughout the entire SiO₂ films.

In Ref. 5, the uniform size distribution of Si nanocrystals (*nc-Si*) in multiple-dose/multiple-energy ion-implanted films was neither verified by Rutherford backscattering (RBS) nor by high-resolution transmission electron microscopy (HRTEM). It was speculated from the observed photoluminescence (PL) band which did not shift with the change of excitation energies. The authors also speculated the PL mechanism in Si nanocrystals as two step processes—it was assumed that the absorption of the incident light took place inside the *nc-Si*, but the emission occurred at the interface of *nc-Si* and the SiO₂ shell surrounding the nanoparticles.

The origin of the PL band in *nc-Si* is still controversial. There is a general consensus that an incident photon in *nc-Si* excites an electron to a higher energy state in the nanocrystal, but the question about the origin of the electron-hole recombination that results in visible light emission remains. Does the recombination occur inside the nanocrystal or at the nanocrystal/SiO₂ interface? Because Si is an indirect band gap semiconductor, a momentum conserving phonon is re-

^{a)}Present address: Nanoscience Technology, Silver Spring, MD; electronic mail: soumenguha@worldnet.att.net

quired for the absorption and emission processes. Therefore, one way to understand the absorption and emission processes in *nc*-Si is to look for the momentum-conserving phonon structures from a resonantly excited *nc*-Si. If the emission occurs inside the nanocrystal, the phonon structures accompanying the PL band would be that of the *nc*-Si; alternatively, if the phonon structures of the Si-O bond at the SiO₂ interface is observed, the emission occurs at the interface. In a recent report by Kanemitsu and Okamata,⁶ PL experiments on resonantly excited *nc*-Si capped with SiO₂ showed that the momentum conserving phonons of the Si-O bond accompanied the PL spectra and concluded that the emission occurred at the *nc*-Si/SiO₂ interface. However, the observed phonon structure was so broad and weak that, in our opinion, these results were far from being conclusive. In *nc*-Si, as the particles get smaller, the phonon modes are broadened and red-shifted.⁷ Observation of this mode for a particle of size around 2 nm as phonon replicas in the PL spectra demands a very carefully monitored experiment with a high density of nanocrystals in the sample. Moreover, it is difficult to reconcile Kanemitsu's model with the quantum confinement model, which has been compiled on the PL band of *nc*-Si in the last five years.⁸ Many researchers favor the quantum confinement model,⁸ i.e., when materials consisting of *nc*-Si are illuminated by incident light, the absorption and emission occur inside the nanocrystal giving rise to an yellow-orange emission around 1.8 eV from a particle of size 2.7 nm. Recently Wolkin *et al.*⁹ claimed the observed PL around 750 nm from oxidized porous Si to have originated at the oxide surface where the carriers were trapped in Si-O bond.

In this study, we re-examined the samples implanted uniformly with Si by Shimizu-Iwayama *et al.*⁵ and addressed a few of the questions discussed in the previous paragraph. We extended the work reported in Ref. 5 by studying the implanted films before and after the anneal treatment with various techniques: (1) Rutherford backscattering (RBS), (2) forward recoil spectroscopy (FRS), (3) small-angle x-ray diffraction (SXR), and (4) high-resolution transmission electron microscopy (HRTEM). The RBS and FRS measurements allowed us to determine the depth distribution of free (i.e., non-oxidized) and oxidized Si and of hydrogen. SXR and HRTEM provided information on the *nc*-Si cluster size distribution inside the SiO₂ films. Three different implanted films with nominally 5, 10, and 15 at % of free Si in SiO₂ films were studied for this investigation. PL studies of the annealed films as a function of excitation wavelength were also conducted. Assuming a log-normal size distribution of Si nanocrystals in the annealed films, the line shapes of the PL spectra as a function of excitation wavelength were calculated. From the fitting of the PL data with calculated line shape, a size distribution for each film was obtained. Since the calculation of the PL line shape assumed a quantum confinement model, a comparison of the size distribution obtained from the PL data with the HRTEM or x-ray data is an indirect test of the application of quantum confinement model to explain the mechanism of PL in *nc*-Si and allows us to compare this model with models proposed by others^{2,6,8,9} to explain the PL mechanism in *nc*-Si.

TABLE I. Order, energies, and fluences for the 5% and 10% implants.

Si ⁺ energy (keV)	5 at % fluence (Si/cm ²)	10 at % fluence (Si/cm ²)
200	5.0×10 ¹⁶	7.5×10 ¹⁶
150	2.5×10 ¹⁶	3.75×10 ¹⁶
100	2.0×10 ¹⁶	3.0×10 ¹⁶
75	7.5×10 ¹⁵	1.125×10 ¹⁶
50	1.25×10 ¹⁶	1.875×10 ¹⁶
25	7.5×10 ¹⁵	1.125×10 ¹⁶
Total Fluence:	1.22×10 ¹⁷	1.84×10 ¹⁷

II. EXPERIMENT

Samples were prepared by implanting Si⁺ ions into a thermally oxidized Si wafer with an oxide thickness of 300 nm. The energy for ion implantation was selected from 25 to 200 keV at varying doses with a beam current of 570 μA. Three films with nominal doses 5, 10, and 15 at % of excess Si were prepared. The specific information on the implantations for the 5 and 10 at % samples is given in Table I. We annealed all three types of samples at 1000 °C in a nitrogen ambient. In order to understand the oxidation of Si particles, two different annealing times were used: one-half and one hour. We studied the following samples with nominal concentrations of added Si: 5 at % (as-implanted, annealed for 0.5 h, and annealed for 1 h), 10 at % (as-implanted, annealed for 0.5 h, and annealed for 1 h), and 15 at % (annealed for 1 h). In spite of a continuous flow of nitrogen in our furnace, we found increased oxidation of the free Si with anneal time, presumably due to the presence of oxygen and/or water vapor contamination in the nitrogen gas.

For the ion-beam analyses of the films, we used 2.3 MeV He⁺ ions for the RBS with the beam incident at 60° from the surface normal and the detector at a backscatter angle of 164° and 2.9 MeV He⁺ ions incident at 75° from the surface normal with a detection angle of 30° for the FRS. The stopper foil located just in front of the FRS detector was a 10.7 μm mylar foil. For both RBS and FRS the beam spots on the specimens were about 2 mm×2 mm. We used our documented spinning-wire dosimetry system to determine the number of helium ions used to generate each spectrum with a precision of ±1, which is quite precise compared to normal RBS measurements and was needed to perform the analyses described below.¹⁰ The program RUMP was used to quantify both sets of results.¹¹

Cross-sectional TEM images of the annealed films were obtained with JEOL electron microscopes (Models JEM 300CX and JEM 4000EX). The contrast in TEM images and lattice fringes were enhanced by an image processing software (NIH Image and Adobe Photoshop). Small-angle x-ray diffraction data from these films were obtained with a Huber four-circle diffractometer that is coupled with a Rigaku rotation anode x-ray generator. The 1.54 Å Cu Kα line was used as a source. The average scan time to record a spectrum was 10 to 12 h.

For the PL experiments, a mixed krypton-argon ion laser, a single monochromator with a cooled charge-coupled device (CCD) array was used. The average laser power used in the visible was about 10 mW focused into a 300 μ spot

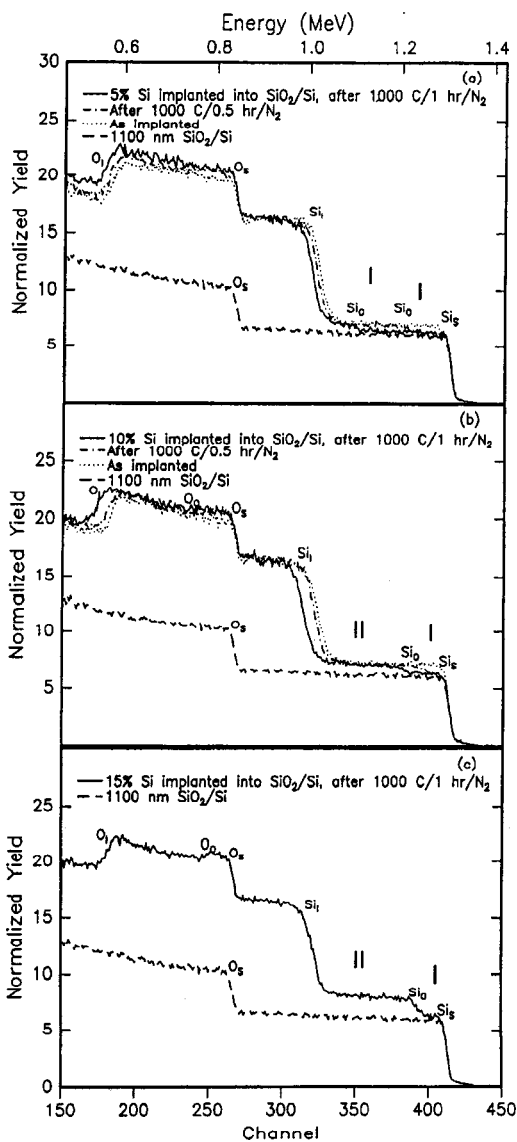


FIG. 1. Comparisons of the Rutherford backscattering spectra for the (a) 5, (b) 10, and (c) 15 at % samples with the 1100-nm-thick thermal fused silica layer on Si. Here I and II refer to oxidized and unoxidized regions.

size on the sample. For the 351 nm UV line, the laser power was about 5 mW.

III. RESULTS AND DISCUSSION

A. Rutherford backscattering (RBS)

Using RBS, we analyzed the following samples with nominal concentrations of added Si: 5 at % (as-implanted, annealed for 0.5 h, and annealed for 1 h), 10 at % (as-implanted, annealed for 0.5 h, and annealed for 1 h), and 15 at % (annealed for 1 h). In addition, we obtained the RBS spectrum from an 1100-nm thick thermal fused silica layer on Si as a control sample.

An overlay of the RBS spectra from the eight different samples and a representative thermal oxide on Si is given in Figs. 1(a)–1(c). Subscripts “S” and “I” refer to the physical location of the indicated element at the surface and at the SiO₂/Si interface, respectively. From these spectra we can conclude that there is added Si in the SiO₂ layer of all the

implanted samples and that the amount increases in the order expected. Detailed examination of the spectra showed that the as implanted samples had essentially uniform concentration of added Si throughout the oxide layer, and the anneals resulted in the oxides being thicker than those of the as-implanted samples. In addition, the amounts of free silicon (i.e., unoxidized Si) was reduced by the anneals, presumably because of oxidation by oxygen and/or water contamination during the anneals in nitrogen. For the annealed samples, the subscript “O” refers to the physical location of the indicated element at the interface between the heavily oxidized (hereafter called oxidized or region I in the text) and slightly oxidized (hereafter called nonoxidized or region II in the text) portions of the added silicon. By comparing the near surface levels of Si in each of the five annealed samples with that for pure SiO₂ on Si, we concluded that there is some small amount of “free” Si in the oxidized portion of the samples.

Detailed RUMP analyses of each of the spectra from the eight samples were completed, and the comparison of the fitted RUMP simulation and the data for the samples annealed for 1 h is presented in Figs. 2(a)–2(c). First order straggling was included as was a scaling of the stopping for Si (i.e., 0.91–0.93, which is consistent with the $\pm 1\%$ precision of the measurements). The fits are quite good except below about channel 225 (i.e., below about 0.7 MeV for the backscattered He), mainly because RUMP does not account for the multiple scattering effects that become more important at lower backscattering energies. The results of all the RUMP analyses of the RBS spectra are summarized in Table II.

From Figs. 1 and 2 and the results summarized in Table II, we can draw several conclusions:

1. Assuming that the initial oxide thickness was 300 nm, very little sputtering occurred during the 5 and 10 at % implants. In unannealed/as-implanted samples, about 10 to 15 nm of oxidized Si layers were observed due to the exposure of samples to air after implantation.

2. The oxide regions of the as-implanted 5 and 10 at % samples contained ~ 1.06 times and ~ 1.09 times, respectively, of the amounts of Si planned for the implants as given in Table I. Furthermore, some of the implanted silicon should have been implanted in the silicon below the oxide layer.

3. The anneals reduced the total amount of free silicon available in the oxide to form nanoclusters due to oxidation of part of the free silicon. For the 5 at % samples the amounts of added free silicon oxidized during the one-half and 1 h anneal steps were 2.7×10^{16} and 7.4×10^{16} Si/cm², respectively. For the 10 at % samples the corresponding amounts of oxidized free silicon were 3.1×10^{16} and 5.4×10^{16} Si/cm², respectively. Thus, comparable amounts of the added free Si were oxidized during the anneals, indicating that the supply of oxygen, not diffusion of the oxygen through the SiO₂, was probably limiting the oxidation process. From the RBS spectra we can conclude that the amount of free silicon was reduced in the oxidized and nonoxidized regions of the oxide layers of all annealed samples. Thus, presumably each of the nanoclusters has oxidized surfaces with the nanoclusters in

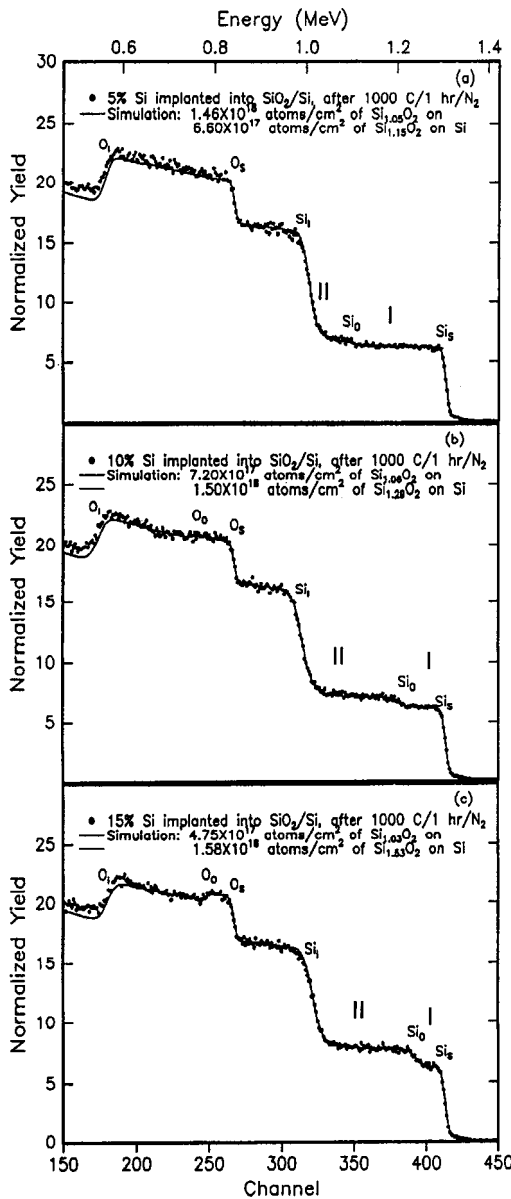


FIG. 2. Representative RUMP simulation analyses for the (a) 5, (b) 10, and (c) 15 at % samples. Here I and II refer to oxidized and unoxidized regions.

the oxidized region having larger oxidized surfaces, thereby reducing the size of the nanocluster.

4. The planned concentration of added free Si was achieved, within ± 1 , only in the nonoxidized layer of each annealed sample. The overall average concentrations of the added free Si were considerably less than the implanted levels, especially after the 1 h anneals.

RBS of the as-implanted 5 and 10 at % samples did not reveal any detectable $Z > 15$ elements; however, all annealed samples had small impurities on the surface and/or in the bulk. The largest impurity on all three annealed samples had a mass like Ti at concentrations of $< 1.5 \times 10^{16}$, 9.8×10^{15} , and 9.5×10^{14} Ti/cm² for the 5, 10, and 15 at % samples, respectively. We do not believe that any of these impurities affected the photoluminescence measurements.

B. Forward recoil spectroscopy (FRS)

We used FRS to assess the surface and bulk levels of hydrogen in the as-implanted and 1 h annealed samples. The

TABLE II. Summary of RUMP analyses of RBS data. (a) Free Si in total oxide refers to the value averaged throughout the total oxide thickness, (b) free Si in nonoxidized layer is related to the layer where only a small fraction of the added Si was oxidized, (c) total thickness is the effective SiO₂ thickness assuming the density for the thermal SiO₂ was 2.19 g/cm³ or 6.6×10^{22} atoms/cm³, (d) oxidized thickness (region I) is the depth corresponding to oxidation of a large fraction of the added Si.

Sample	Free Si in total oxide		Free Si in nonoxidized layer		Layer thickness	
	cm ²	at%	cm ²	at%	total nm	oxidized nm
5% as-implanted	1.29×10^{17}	6.49	1.29×10^{17}	6.83	283	15
5% annealed, 0.5 h	1.02×10^{17}	5.00	9.06×10^{16}	6.25	295	89
5% annealed, 1 h	5.54×10^{16}	2.61	3.14×10^{16}	4.76	313	218
10% as-implanted	2.00×10^{17}	10.0	2.00×10^{17}	10.4	272	12
10% annealed, 0.5 h	1.68×10^{17}	8.18	1.68×10^{17}	9.91	287	55
10% annealed, 1 h	1.46×10^{17}	6.59	1.32×10^{17}	8.81	314	107
15% annealed 1 h	2.42×10^{17}	11.8	2.37×10^{17}	15.0	275	71
15% annealed 1 h	2.50×10^{17}	11.9	2.46×10^{17}	15.3	280	74

largest of the surface hydrogen peaks corresponded to 1.9×10^{16} H/cm² and was found on the 5 at % as-implanted sample. The amounts of hydrogen found ($4.5 - 19 \times 10^{15}$ H/cm²) on these surfaces are typical of those found on all but the most carefully treated and handled samples. With one exception, the concentration of hydrogen in the SiO₂ layer was about 230 at ppm. The only anomaly occurred for the 5 at % annealed sample that had a buried, 180-nm thick layer of 0.22 at % hydrogen in SiO₂ that was centered about 190 nm from the surface. Although the origin of this layer is not clear, the low level of hydrogen found in all these samples did not affect the RBS analysis and should not affect the photoluminescence measurements.

C. High-resolution transmission electron microscopy (HRTEM)

We performed HRTEM on the three samples annealed for 1 h. In Fig. 3, we show cross-sectional TEM images of the 15 at % Si sample as annealed for 1 h. Figure 3(a) is a typical low-magnification image and, as for all three samples

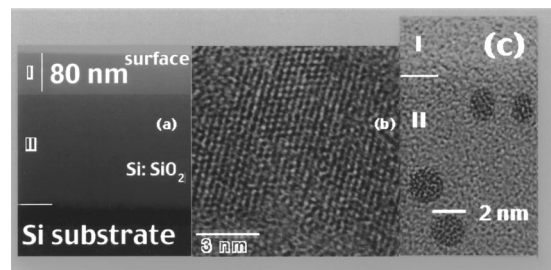


FIG. 3. Cross-section TEM images of a 15 annealed sample. (a) Three regions are shown: (I) heavily oxidized SiO₂ layer where small Si clusters (< 2 nm) were seen, (II) Si clusters of sizes 1 and 3 nm in the SiO₂ layer, and the third region is the Si substrate. (b) Very large particles were detected near the substrate. (c) Smaller particles between 1 and 3 nm were found in regions I and II.

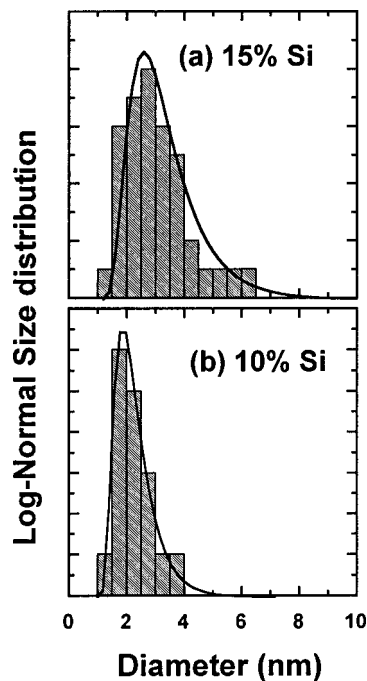


FIG. 4. Log-normal size distributions (solid curve) using Eq. (8) of Ref. 1 and histograms (shaded area) showing the measured size distributions from TEM analyses for two samples: (a) 15 at % Si, (b) 10 at % Si.

annealed for 1 h, we observed defined regions of differing contrast in the SiO₂ matrix as indicated by I and II in this figure. The depth of region I in the 15 at % samples is, approximately, 80 nm, which is consistent with the RBS result of 71 nm given in Table II. This is the region that was heavily oxidized in the annealing process presumably due to the presence of oxygen contamination in the nitrogen gas. As a result, a large fraction of the added Si and/or Si nanoparticles became oxidized in region I. Very large particles of sizes >5 nm were observed in contact with the Si substrate as shown by Fig. 3(b) in all three samples annealed for 1 h. Using high magnification, we found Si particles with an average diameter of ~2.5 nm throughout region II as shown by Fig. 3(c). The average particle size was found to be smaller, around 1–2 nm in the region I, and such particles were observed throughout the entire region for the 15 and 10 at % annealed samples. Apparently oxidation during annealing limited the growth of the Si nanocrystals. We try to estimate the size distribution from the HRTEM images in two samples, which are shown in Figs. 4(a) and 4(b). For each sample, a histogram is obtained by counting about 50–100 particles in regions I and II as shown by Fig. 3(a). They were fitted with log-normal distribution curves shown by solid lines in Figs. 4(a) and 4(b).

D. Small-angle x-ray diffraction (SXR)

Figure 5 shows SXR intensities from the 15 (1 h anneal) and 10 at % (1/2 h anneal) Si samples as a function of particle size. The sizes (D) were obtained from the scattering angle 2θ with the relationship: $2D \sin \theta = \lambda$, where λ is the x-ray wavelength (1.54 Å). Each sample showed two broad size distributions: one around 6–7 nm and the other around

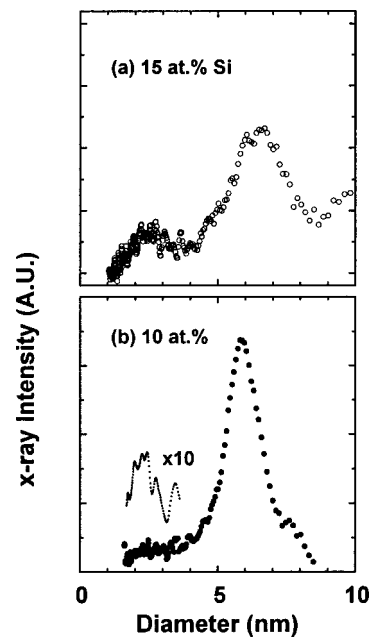


FIG. 5. Small-angle x-ray diffraction intensity as a function of particle size from (a) 15 at % (1 h anneal) and (b) 10 at % (1/2 h anneal). A sloping background has been subtracted from each spectrum.

2–3 nm. Although our HRTEM measurements did not show particles larger than 3 nm in the SiO₂ matrix except near the substrate, SXR data showed higher intensities for the larger particles, probably because of their large volumes as compared to the smaller particles. Because a sloping background was subtracted from the raw data, the Peak heights of these two size distributions should not be regarded as a true measure of their intensities. We did not detect any x-ray intensity from the 5 at % (0.5 h anneal) sample, probably due to its low concentration of free Si, as shown by the RBS results in Table II.

It has been established⁴ that the band gap of Si particles larger than 4 nm is that of bulk Si, which is 1.1 eV. One should not expect the quantum confined excitonic states, that would give rise to visible photoluminescence, to exist in particles larger than 4 nm. But we must point out that these large Si particles may contain morphological defects, Si dangling bonds, and color centers that may produce midgap states in the SiO₂ matrix; a visible PL spectrum from these defects might be observed that normally occur at the oxide interface and often, misconstrued as the visible emission associated with Si nanocrystals.

E. Photoluminescence (PL)

Figure 6 shows the PL spectra from three annealed samples taken at several excitation wavelengths. Except for a slight reduction in PL intensity shown in Figs. 6(b) and 6(c), essentially the same PL spectra were found for the 5 and 10 at % samples after annealing for one hour. This implies that the effect of a longer anneal time is to decrease the concentration of Si clusters, presumably due to increased oxidation. This decrease of PL intensity as a function of anneal time was also observed for a single-dose/single-energy implant which we have reported elsewhere.³

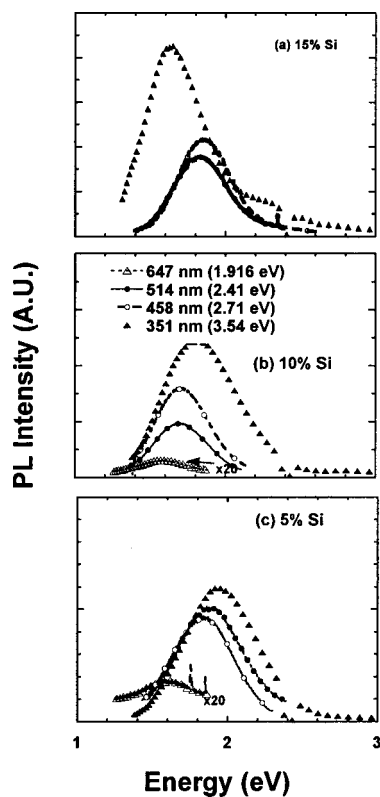


FIG. 6. Photoluminescence spectra from (a) 15 (1 h anneal), (b) 10 (1/2 h anneal), and (c) 5 at % (1/2 h anneal) samples. These spectra are the raw data and are not corrected for the instrument response.

For the 351 nm excitation, we observed a blue-shift of the PL peak energy with decreasing fluences, indicating a decrease in cluster size that results in a change of the band gap of Si. However, the shift of the 15 at % annealed sample as a function of excitation wavelength is different than that of the other two annealed samples. In a site-selective process, higher (lower) excitation energies (wavelengths) would select particles of smaller sizes and, hence, the PL peak energy should appear at higher energies as compared to lower (higher) excitation energies (wavelengths). Although we observed such a trend for the 10 and 5 at % annealed samples, the PL spectra of the 15 at % annealed sample shifted to the red at shorter wavelengths. This anomaly may be due to a broader size distribution in this sample as evidenced by SXRD. In order to understand this unusual trend in the 15 at % Si sample, we next try to calculate the particle size distribution from the PL spectra taken at two excitation energies.

Assuming that the PL originated inside the nanocrystal and the shift of the PL band is due to quantum confinement of excitons in nanocrystals, the size distribution in these samples are estimated from the PL spectra in the following manner. In a previous report¹² we calculated the PL spectra from the size distribution following a phenomenological theory developed by Yorikawa and Muramatsu.¹³ In this theory, it was assumed that the energy gap (E_g) varied with size D of nanocrystals as $1/D^{1.25}$. In addition, a single log-normal size distribution was assumed in this model to calcu-

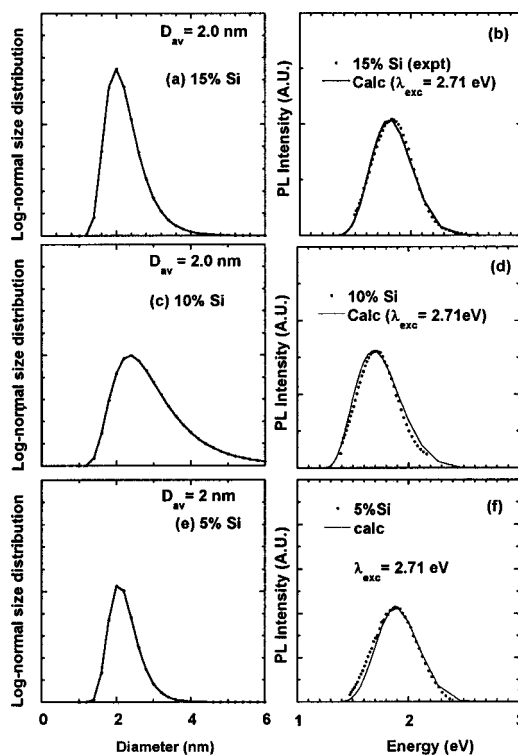


FIG. 7. Size distributions (a), (c), and (e) are used to calculate the line shape spectra (solid lines) for the (b) 15, (d) 10, and (f) 5 at % Si samples of Fig. 5, respectively. Selected datapoints of the experimental PL spectra taken at an excitation energy of 2.71 eV are shown by the filled circles. PL spectra are corrected for the instrument response.

late the line shape of a PL spectrum at excitation energies between 1.96 and 4.88 eV. According to this model, for a nanocrystal with a log-normal size distribution of an average size D , the line shape of a PL spectrum would change as a function of excitation wavelength (energy). Therefore, once one determines the size distribution in a sample, one can calculate line shapes of PL spectra for a certain cluster size D at all excitation wavelengths (energies). We tried a similar approach to calculate the PL spectra for 5, 10, and 15 at % annealed Si samples at two excitation energies, 2.71 and 3.54 eV.

In Ref. 13, the authors used a single size distribution to fit the experimental PL data at excitation energies between 1.96 and 4.88 eV. The particle size distribution in the samples from which the PL data were taken was assumed, but never measured. Using this model, we were unable to fit the PL data at all excitation energies between 1.96 and 3.54 eV with our measured size distributions in two samples shown by Fig. 4. In our fitting process, we used the same log-normal size distribution for each sample, shown by Figs. 4(a) and 4(b), to fit the PL data at the excitation energy of 3.54 eV for the 15 at % and 10 at % Si (Fig. 8). When we tried to use the same size distribution to fit the PL data at the excitation energy 2.71 eV, we got a poor fit. Therefore, we used a slightly different size distribution (Fig. 7) to fit the PL data at excitation energies between 1.96 and 2.71 eV for these samples.

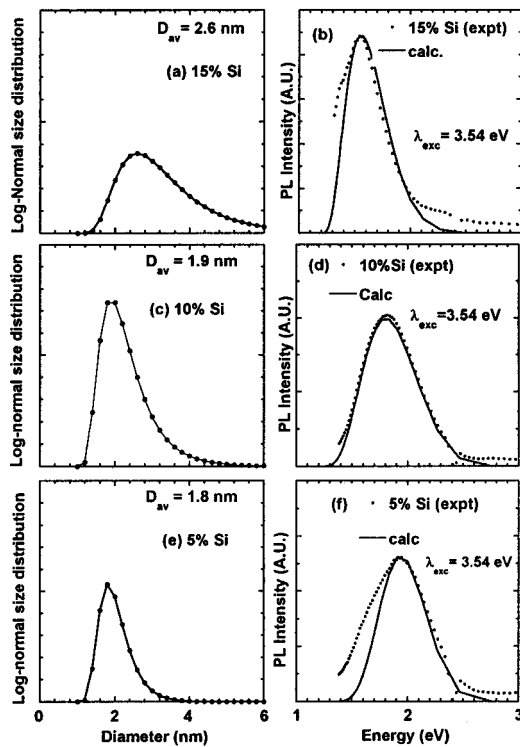


FIG. 8. Size distributions (a), (c), and (e) are used to calculate the line shape spectra (solid lines) for the (b) 15, (d) 10, and (f) 5 at % Si-samples, respectively. Selected datapoints of the experimental PL spectra taken at an excitation energy of 3.54 eV are shown by the filled circles. PL spectra are corrected for the instrument response.

We believe that for lower excitation energies, only the emission from nanoparticles of larger sizes were detected due to their larger band gaps,^{4,14} therefore from the entire size distribution shown by Fig. 4, particle sizes that contribute to the PL spectra at these excitation energies are reflected in the size distribution shown by Figs. 7(a), 7(c), and 7(e). These size distributions were used to calculate the line shapes of the PL spectra of the three annealed samples shown by the solid lines in Figs. 7(b), 7(d), and 7(f) and the experimental PL data are shown by the filled circles. Interestingly enough, the average diameter obtained from this fitting procedure is the same for all three samples, but with a slightly different size distribution. According to van Buuren *et al.*,⁴ the band gap for a 2 nm particle is, approximately, 1.9 eV and hence the observed PL from the 5 at % sample could be assigned to the band-edge emission from the quantum-confined excitonic states of Si nanocrystal of size 2 nm. Note that the 15 and 10 at % Si samples do not show the PL peaks at 1.9 eV although the average particle size is the same for all three samples. Our calculation indicates that a broader size distribution would shift the PL band irrespective of the mean diameter. Therefore, the quantum-confinement model interpretation of the PL mechanism still holds for the 15 and 10 at % annealed Si samples.

When these samples were excited by the 351 nm (3.54 eV) laser line, as shown by Figs. 8(b), 8(d), and 8(f), the PL peak shifted to the blue with decreasing particle size in the three samples as shown by the size distribution in Figs. 8(a), 8(c), and 8(e). We conclude that the observed PL spectra

from these samples are the band-edge emissions from Si particles of average sizes 2.6, 1.9, and 1.8 nm; the PL peaks agree quite well with the absorption edges for these sizes reported in Ref. 4. We, therefore, have shown another approach to interpret the PL data as compared to the qualitative surface state model used in Refs. 5 and 9.

Finally, we try to compare our PL data with the observed red PL around 1.9 eV in oxidized porous Si,⁹ in which the authors claimed that the observed red PL was due to exciton recombination at the oxide surface. This interpretation was based on a theoretical calculation of electronic states of Si clusters passivated by either hydrogen or oxygen atoms using a self-consistent tight-binding method. In this calculation, as the particle size (D) became smaller, the Si band gap became larger due to quantum confinement and obeyed a relationship: $E_g \sim 1/D^{1.33}$.¹⁴ When Si clusters were passivated by oxygen, trapped states due to Si–O bond appeared in the band gap of Si clusters of sizes less than 3 nm. Therefore, the authors opined that the electron–hole recombination must occur via these trapped states created due to oxygen passivation of the Si clusters. As a result the PL peak should not be blue-shifted in accord with the $1/D^{1.33}$ law and this observation was reported in Ref. 9.

Our analyses were based on three sizes of average diameter 2.6, 1.9, and 1.8 nm that belonged to zone II of Ref. 9. In this zone, the band gaps of the hydrogen- and oxygen-passivated Si clusters of sizes between 1.8 and 3 nm were comparable; therefore our PL data could not test the oxide model of Ref. 9. Neither can we rule out the surface state recombination of excitons as the origin of red emission from Si clusters heavily coated with oxides. One needs more sizes between 1 and 3 nm with a narrow size distribution to test the oxide model of Ref. 9.

IV. SUMMARY AND CONCLUSION

In summary, we have demonstrated that multiple dose/multiple energy ion implantation can be used to grow Si nanoparticles of reasonably uniform size. We have determined by RBS the amount of excess, ion-implanted Si in the SiO₂ matrix before and after annealing. RBS showed that in the first 55–218 nm of the 300 nm SiO₂ films, most of the added Si was oxidized during the annealing process. We have also found, by HRTEM, Si particles of varying sizes between 1 and 3 nm in the remainder of the SiO₂ films. Very large Si particles have been found near the substrate. We conclude that to grow a narrower size distribution, one should start with added Si less than 10 at %, and we found it difficult to control the size distribution with added Si greater than 10 at %. We have calculated the line shape spectra with measured size distributions that fit the PL spectra from the three samples using a phenomenological model that invokes quantum confinement of excitons in *nc*-Si. The band gap energy and the average particle size obtained from the calculated line shape spectra agree well with the quantum confinement model. However, as regard to the origin of the PL spectra in Si nanocrystals we need to grow Si particles with

narrow size distribution to answer the question whether the exciton recombines inside the nanocrystal or at the oxide coated Si nanocrystal surface.

ACKNOWLEDGMENTS

It is a pleasure to acknowledge useful discussions with T. E. Felter and L. L. Chase of Lawrence Livermore National Laboratory. The LLNL part of this work was performed under the auspices of the U. S. Department of Energy by the Lawrence Livermore National Laboratory under Contract No. W-7405-ENG-48.

¹D. J. Lockwood, Z. H. Lu, and J.-M. Baribeau, *Phys. Rev. Lett.* **76**, 539 (1996).

²L. N. Dinh, L. L. Chase, M. Balooch, W. J. Siekhaus, and F. Wooten, *Phys. Rev. B* **54**, 5029 (1996).

³S. Guha, M. D. Pace, D. N. Dunn, and I. L. Singer, *Appl. Phys. Lett.* **70**, 1207 (1997); and references therein.

⁴T. van Buuren, L. N. Dinh, L. L. Chase, W. J. Siekhaus, and L. J. Terminello, *Phys. Rev. Lett.* **80**, 3803 (1998).

⁵T. Shimizu-Iwayama, N. Kurumado, D. E. Hole, and P. D. Townsend, *J. Appl. Phys.* **83**, 6018 (1998).

⁶Y. Kanemitsu and S. Okamoto, *Phys. Rev. B* **58**, 9652 (1998).

⁷S. Guha, P. Steiner, and W. Lang, *J. Appl. Phys.* **79**, 8664 (1996).

⁸A. G. Cullis, L. T. Canham, and P. D. J. Calcott, *J. Appl. Phys.* **82**, 909 (1997).

⁹M. V. Wolkin, J. Jorne, P. M. Fauchet, G. Allan, and C. Delrue, *Phys. Rev. Lett.* **82**, 197 (1999).

¹⁰R. G. Musket, R. S. Daley, and R. G. Patterson, *Nucl. Instrum. Methods Phys. Res. B* **83**, 425 (1993).

¹¹Computer Graphics Service, Lansing, New York (1989), a commercially available version of L. R. Doolittle, *Nucl. Instr. Meth.* **9**, 344 (1985).

¹²S. Guha, *J. Appl. Phys.* **84**, 5210 (1998).

¹³H. Yorikawa and S. Muramatsu, *Appl. Phys. Lett.* **71**, 644 (1997).

¹⁴J. P. Proot, C. Delrue, and G. Allan, *Appl. Phys. Lett.* **61**, 1948 (1992).